

Size Effects of Hardness and Strain Rate Sensitivity in Amorphous Silicon Measured by Nanoindentation



DARIUSZ M. JARZĄBEK, MICHAŁ MILCZAREK, SZYMON NOSEWICZ,
PIOTR BAZARNIK, and HELMUT SCHIFT

In this work, dynamic mechanical properties of amorphous silicon and scale effects were investigated by the means of nanoindentation. An amorphous silicon sample was prepared by plasma-enhanced chemical vapor deposition (PECVD). Next, two sets of the samples were investigated: as-deposited and annealed in 500 °C for 1 hour. A three-sided pyramidal diamond Berkovich's indenter was used for the nanoindentation tests. In order to determine the strain rate sensitivity (SRS), indentations with different loading rates were performed: 0.1, 1, 10, 100 mN/min. Size effects were studied by application of maximum indentation loads in the range from 1 up to 5 mN (penetrating up to approximately one-third of the amorphous layer). The value of hardness was determined by the Oliver–Pharr method. An increase of hardness with decrease of the indentation depth was observed for both samples. Furthermore, the significant dependence of hardness on the strain rate has been reported. Finally, for the annealed samples at low strain rates a characteristic “elbow” during unloading was observed on the force-indentation depth curves. It could be attributed to the transformation of (β -Sn)-Si to the PI (pressure-induced) a-Si end phase.

<https://doi.org/10.1007/s11661-020-05648-w>
© The Author(s) 2020

I. INTRODUCTION

THE use of thin films in many branches of modern industry, *i.e.*, in photonics, micro- and nanoelectronics, and micro- and nano-electromechanical systems (MEMS and NEMS), has generated a strong interest in their mechanical properties. The requirements for mechanical reliability and durability become more crucial with increasing the complexity of the systems. Amorphous silicon (a-Si) is one of the most common materials used for manufacturing of MEMS.^[1,2] In the literature, one can find evidence that processing conditions like deposition temperature, pressure, and flow rate of gases and processes like etching, chemical treatments, or ion implantation are known to affect the microstructural features as well as the distribution of volume and surface defects in this material.^[3–5] To gain

a deeper understanding between processing-structure-property-performance relationship for a-Si, much recent research interest has focused on characterizing hardness, Young's modulus, and pressure-induced phase transformations measured, *i.e.*, by nanoindentation.^[3,5–7] This measurement method is particularly dedicated and successfully applied for studying of mechanical properties of thin films.^[8–11] For example, Kiran *et al.* performed high-temperature nanoindentation on pure ion-implanted amorphous silicon.^[5] They shown that unrelaxed a-Si deforms entirely *via* plastic flow, whereas a clear transition in the mode of deformation is observed in an annealed a-Si. Furthermore, Haberl *et al.* studied the deformation behavior of a-Si using spherical nanoindentation^[7] and again observed phase transformations only in the annealed sample. It should also be noted that the phase transformation was different for different unloading rates. Furthermore, the issue of indentation-induced phase transformations in silicon has been widely studied.^[12–15] Unfortunately, the problem of dependence of mechanical properties, *i.e.*, hardness of a-Si on indentation depth or strain rate, can rarely be found in the literature.

One of the parameters that indicate the dynamic behavior of the material is the strain rate sensitivity (SRS). In the literature, one can find many papers about measuring SRS of different materials with split Hopkinson bar.^[16,17] On the other hand, thin films cannot be investigated with this technique. Fortunately,

DARIUSZ M. JARZĄBEK is with the Institute of Fundamental Technological Research, Polish Academy of Sciences, 02-106 Warsaw, Poland and also with the Institute of Fundamental Technological Research, Polish Academy of Sciences, Pawinskiego 5B, 02-106 Warsaw, Poland. Contact e-mail: djarz@ippt.pan.pl MICHAŁ MILCZAREK and SZYMON NOSEWICZ are with the Institute of Fundamental Technological Research, Polish Academy of Sciences. PIOTR BAZARNIK is with the Warsaw University of Technology, 00-661 Warsaw, Poland. HELMUT SCHIFT is with the Paul Scherrer Institut, 5232 Villigen PSI, Switzerland.

Manuscript submitted September 24, 2019.
Article published online February 3, 2020

the nanoindentation can also be useful for SRS determination. This technique offers hardness measurement with constant strain rates at a small scale. It should be mentioned that classical nanoindentation is not dedicated to dynamic measurements but the most advanced nanoindenters are equipped with high-performance electronics, which allows to apply loads and collect data with high speeds.

It is generally accepted that the values of SRS are strongly size-dependent: for face-centered-cubic (fcc) metals, SRS normally increases with decreasing grain sizes, whereas the opposite holds for body-center-cubic (bcc) structures.^[18] In contrast, amorphous, metallic glasses exhibit high strength, wear, and corrosion resistance,^[19] but their deformation is shear band controlled; hence, they are generally brittle and their SRS is close to zero.^[20,21] On the other hand, a-Si is different from amorphous metallic glasses due to the highly directional covalent bonding that can make deformation processes more complex. Understanding the pressure-induced deformation in a-Si is not only important from the scientific point of view but also it is also relevant for a number of applications, *i.e.*, photovoltaic cells and MEMS.^[22,23] Unfortunately, there are many ‘forms’ of a-Si and its structural ordering, morphology, and impurity content vary considerably depending on its formation method and thermal history. Therefore, in this paper we perform nanoindentation tests with different strain rates and depths on two samples: as-deposited and annealed, in order to study dynamic properties and size effects in probably the most popular a-Si films prepared by PECVD.^[24,25]

II. EXPERIMENTAL

A. Samples Preparation

In this work, mechanical properties of amorphous silicon were investigated by the means of nanoindentation. An amorphous silicon sample was prepared at the Paul Scherrer Institute by PECVD (plasma-enhanced chemical vapor deposition) in the following way. As substrate a blank 100 mm Si $\langle 100 \rangle$ wafer was used. A chamber and the substrate were pre-cleaned with N_2O for 3 minutes with a flow of 710 sccm, pressure of 1000 mTorr, temperature of 250 °C, and with HF power of 20 W. Then a deposition gas was introduced to the chamber, as a 5 pct of SiF_4 in N_2O , and a flow stabilized at the level of 500 sccm with a chamber pressure of 1000 mTorr and temperature of 250 °C. Deposition was done with HF power of 20 W and lasted for 10 minutes. As the last step, the whole chamber was purged with N_2 gas. Before experiments the wafer was cut into smaller specimens. Some of them were annealed before nanoindentation in 500 °C for 1 hour, others were investigated as-deposited.

The samples were studied to obtain microstructural properties with the use of transmission electron microscope (TEM) Jeol 1200, operating under accelerating voltage of 120 kV. The samples were cut using the focussed ion beam (FIB) technique, with a Hitachi

NB5000 microscope. The samples do not differ in structure. Moreover, to confirm the presence of amorphous regions selected area electron diffraction (SAED) was used.^[26] Figure 1(a) shows SAED image taken from interfacial regions confirmed the presence of amorphous layer (blurred diffraction rings) on the crystalline $\langle 001 \rangle$ Si substrate (diffraction spots with a 001 zone axis).

Due to the fact that the thickness of the coatings could vary in different positions at the wafer, it was determined according to the following procedure. After the indentations with small forces, an indentation test with a relatively high force equal to 30 mN was performed in a distance of about 20 μm . Since nanocrystalline silicon is brittle, a part of the coating was split off and flown free (Figure 1(b)). Next, the created structure was measured by an atomic force microscope (Nanosurf Flex AFM) (Figure 1(c)). The thickness of the coating was determined as a difference between the surface of a nanocrystalline film and the surface of single-crystal silicon. An example profile is shown in Figure 1(d). We have taken into consideration only the results obtained in the center of the wafer where the coating thickness was equal to 510 ± 5 nm (the average obtained from all the experiments).

B. Nanoindentation

The nanoindentation of the samples was performed on an Ultra Nanoindentation Tester (UNHT Anton Paar). The device exhibits an extremely low thermal drift^[27] which is of particular importance in long, strain rate sensitivity measurements.^[28] It is due to the fact that the principle of the UNHT is based on the idea of using two independent vertical axes: one axis is dedicated to the indentation measurement itself and the other axis is used for active top referencing (Figure 2). The system can be considered as two nanoindentation systems, which are intimately linked: one responsible for active top referencing of the sample surface and the other for performing the indentation. Hence, all thermal dilatation of the sample and the frame are simply disregarded because of the fact that the displacement of the indenter is measured with respect to the reference, load of which is independently controlled—the reference is ‘‘floating’’ on the sample surface.

Nanoindentation was performed by the nanoindentation tester equipped with a three-sided pyramidal diamond Berkovich’s indenter. In order to determine SRS, indentations with different loading rates were performed: 0.1, 1, 10, 100 mN/min. Size effects were studied by application of maximum indentation loads in the range from 1 up to 5 mN (penetrating up to approximately one-third of the amorphous layer^[7]). The value of hardness was determined by the Oliver–Pharr method. It is a standard procedure for determining hardness from the nanoindentation load–displacement curves. The projected contact area between indenter tip and sample can be estimated by the depth of impression obtained from a load–displacement curve. The hardness is determined by dividing the load by the area of contact. On the other hand, one can determine the projected contact area by direct measurement. It is

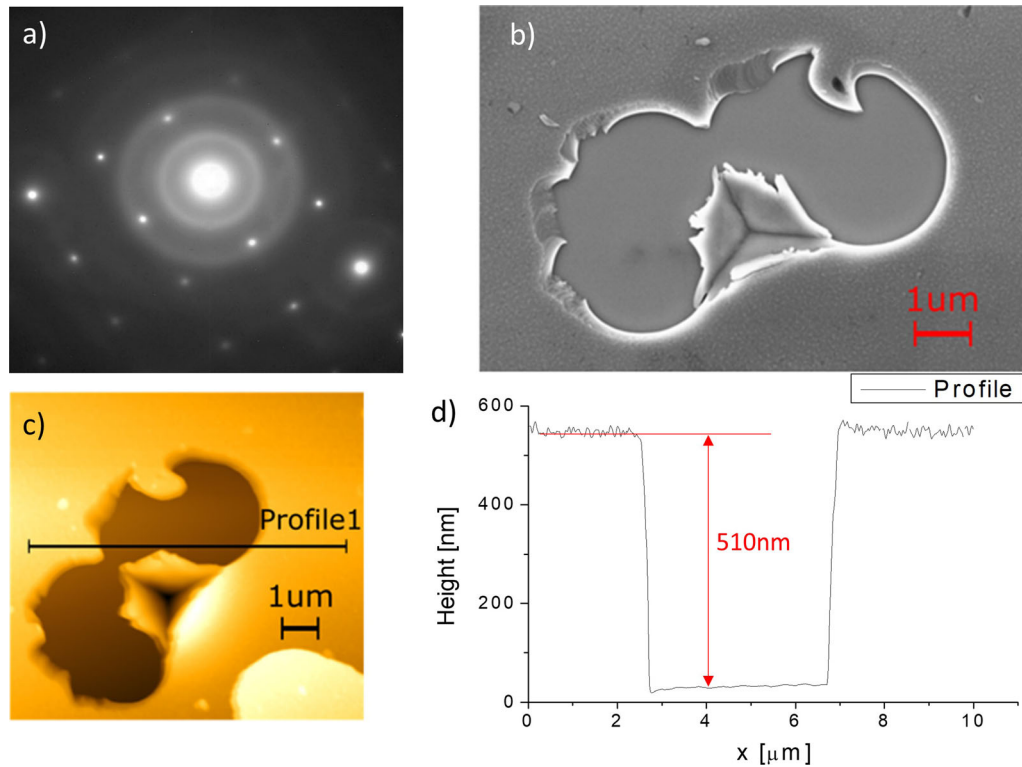


Fig. 1—(a) SAED image taken from this region showing blurred rings stemming from the amorphous layer. (b) SEM micrograph of a spot where the a-Si coating on top of the silicon substrate was split off; (c) AFM topography plot and (d) profile of the defect indicating the thickness of the coating.

recommended in the case of high pile-ups or significant thermal drift (Figure 3(a)). We have applied the latter approach to verify the results obtained by the Oliver–Pharr method and to confirm the high thermal stability of our nanoindenter. The indentation imprints were measured by AFM (Figure 3(b)). The real projected contact area was then evaluated by applying the algorithms available in Gwyddion software (Figure 3(c)).

C. Determination of Strain Rate Sensitivity

Strain rate sensitivity (SRS) provides information about the influence of strain rate on material properties such as hardness. In the case of bulk materials, the tensile tests are used for SRS determination. It is then defined as the change in the yield stress or tensile strength $\frac{\sigma}{\sigma_0}$ divided by the change in the uniaxial strain rate $\frac{\dot{\epsilon}}{\dot{\epsilon}_0}$ at a constant temperature using the following equation:

$$m = \frac{\partial \ln \frac{\sigma}{\sigma_0}}{\partial \ln \frac{\dot{\epsilon}}{\dot{\epsilon}_0}} \quad [1]$$

On the other hand, for nanoindentation, SRS is determined as follows^[18]:

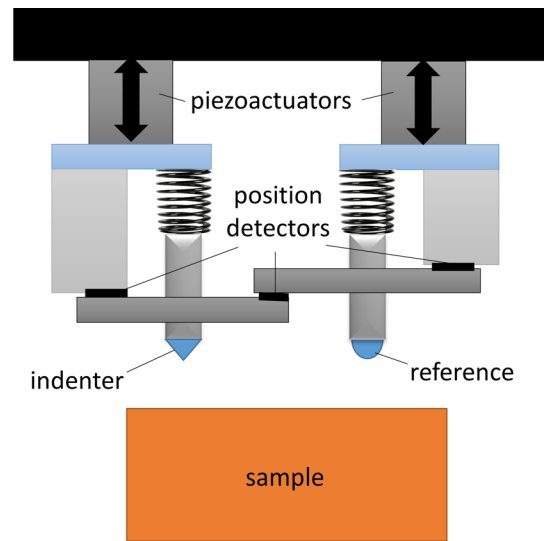


Fig. 2—A scheme of the nanoindentation device used in this study.

$$m_{\text{ind}} = \frac{\partial \ln H}{\partial \ln \dot{\epsilon}_i} \quad [2]$$

where H is the hardness and $\dot{\epsilon}_i$ is the indentation strain rate, which according to Reference 29

$$\dot{\epsilon}_i = \frac{\dot{P}}{2P}. \quad [3]$$

In this work, we have plotted $\ln H$ vs $\ln \dot{\epsilon}_i$ and performed the linear fit. SRS is then equal to the slope of the fitted straight line (Figure 4).

III. RESULTS

The exemplary load–displacement curves for two amorphous silicon samples—as-deposited and annealed—are shown in Figure 5. The curves were obtained at various loading rates starting from 100 down to 0.1 mN/min from samples loaded to 5 mN. In the case of as-deposited sample (Figure 5(a)), both loading and unloading portions are smooth without any discontinuities suggesting homogeneous deformation. The quantitative data obtained from the above curves and curves obtained for 1 mN max load are given in Table I. We observe that the maximum penetration depth h_{\max} decreases with the loading rate in both cases. Similarly, the residual depth h_p also decreases with increasing loading rate.

In contrast, the indentation curves obtained from the annealed a-Si sample under similar experimental conditions shown in Figure 5(b) are significantly different. Firstly, the sample is slightly softer. Secondly, the unloading curves obtained from indentation with the loading rates equal to 1 and 0.1 mN/min exhibit a so-called elbow behavior. The information from the load–displacement curves is quantitatively confirmed by the data presented in Table II. Similarly to as-deposited sample, h_{\max} decreases with the loading rate for both 5 and 1 mN max load. However, h_p for both cases start to decrease for loading rates equal to 1 and 0.1 mN/min. This suggests different modes of elastic recovery or phase transformation on unloading.

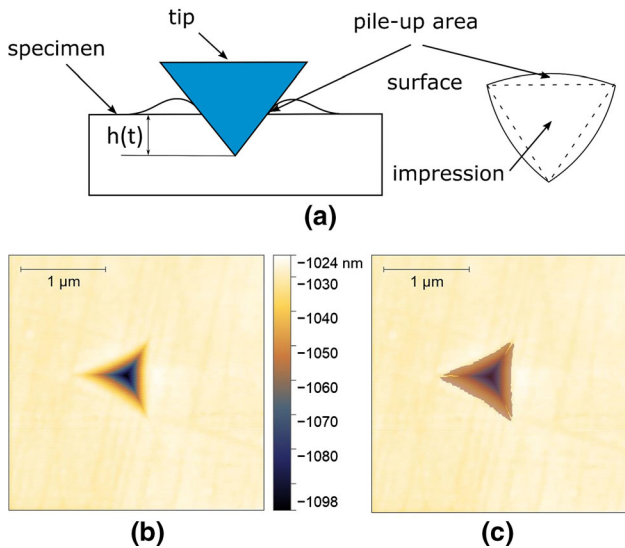


Fig. 3—(a) Schematic of the indentation of a three-sided pyramidal tip into the surface. (b) AFM topography plot of the indentation and (c) processed micrograph.

The results of hardness and indentation modulus measurement of the two samples are shown in Figure 6. The hardness in almost every case is higher for the as-deposited sample. There are just two exceptions but the difference is within the measurement error. It is also apparent that for both samples hardness significantly depends on the loading rate. In both cases, the highest hardness values are obtained for the highest loading rate, which is equal to 100 mN/min. The evidence suggests the occurrence of a size effect—the hardness depends on applied load/indentation depth.^[30–32] This effect is clearly visible for the highest loading rate but is less significant in the case of lower loading rates. For example, in the case of the as-deposited sample the difference between measured hardness values obtained for 1 and 5 mN max load is equal to 3200 MPa when the loading rate is 100 mN/min and to 1000 MPa when the loading rate is 0.1 mN/min. A similar effect is observed for the annealed sample.

The indentation modulus also decreases with the applied load/indentation depth. However, the decrease is significantly stronger for the annealed sample. For each loading rate, for 1 mN max load the value of the indentation modulus is higher for the annealed sample. On the other hand, for 5 mN max load it is usually higher for the as-deposited sample. Similarly to the hardness, the indentation modulus decreases also with the decrease of the loading rate. The only exception occurs for the lowest loading rate (0.1 mN/min). A significant jump of the indentation modulus has been observed for both investigated samples.

Furthermore, one can determine the indentation strain rate according to Eq. [3] and then plot hardness vs indentation strain rate as it is shown in Figure 7(a). It should be noted that when the indentation strain rate is plotted on a logarithmic scale, the linear relation between hardness and logarithm of strain rate can be postulated. The coefficient of determination is equal to 0.94 and 0.89 for the as-deposited and annealed samples, respectively. Furthermore, in Figure 7(b) a plot of SRS vs max load is shown. In general, SRS is higher for the as-deposited sample and it is independent of max load for higher loads. However, a significant increase of SRS

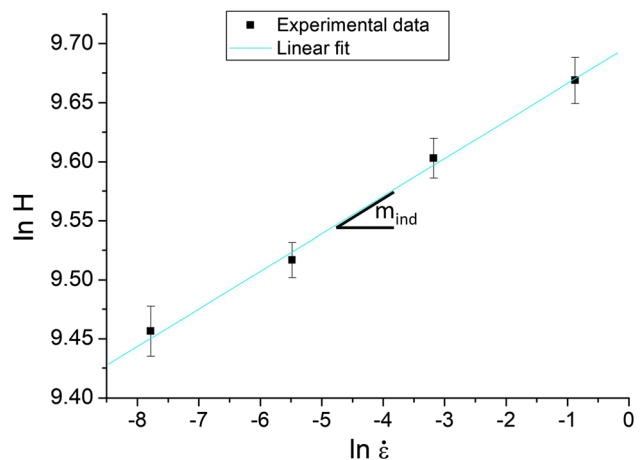


Fig. 4—An example $\ln H$ vs $\ln \dot{\epsilon}$ plot for SRS determination.

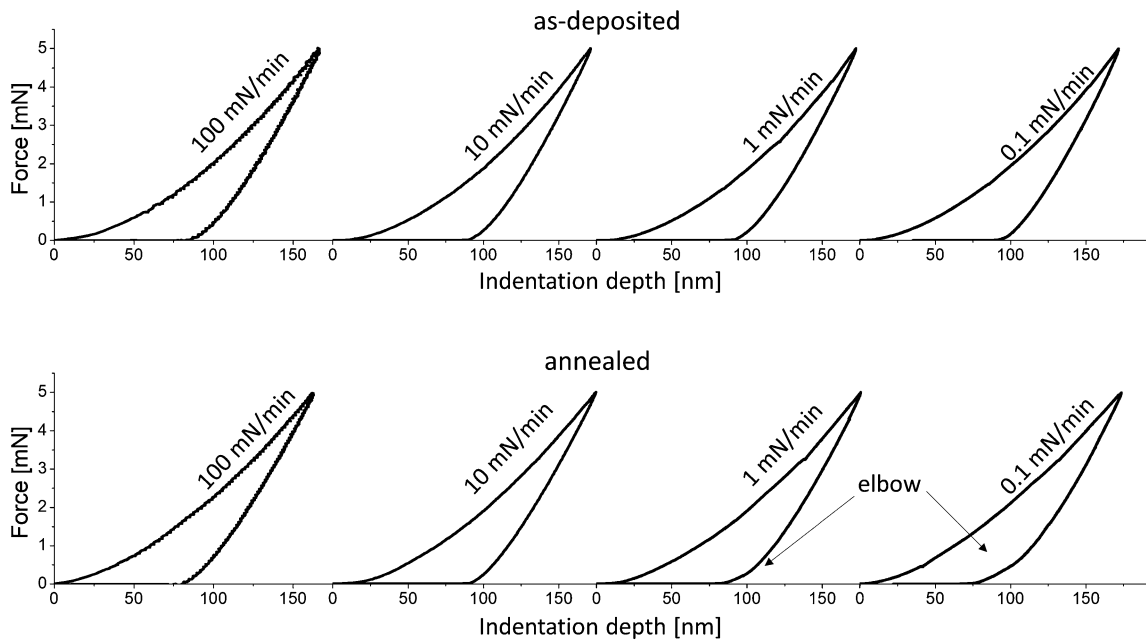


Fig. 5—Indentation curves.

Table I. The Data Obtained from the P-h Curves for 1 and 5 mN Max Load (As-deposited Sample)

| Loading Rate (mN/min) | As-deposited Sample | | | |
|-----------------------|---------------------|------------|-----------------|------------|
| | Max Load: 1 mN | | Max Load: 5 mN | |
| | h_{\max} (nm) | h_p (nm) | h_{\max} (nm) | h_p (nm) |
| 100 | 60 ± 1 | 21 ± 3 | 161 ± 4 | 79 ± 5 |
| 10 | 65 ± 2 | 26 ± 2 | 168 ± 4 | 84 ± 6 |
| 1 | 66 ± 2 | 27 ± 3 | 169 ± 4 | 86 ± 8 |
| 0.1 | 67 ± 2 | 29 ± 1 | 174 ± 4 | 93 ± 6 |

Table II. The Data Obtained from the P-h Curves for 1 and 5 mN Max Load (Annealed Sample)

| Loading Rate [mN/min] | Annealed Sample | | | |
|-----------------------|-----------------|---------------|-----------------|---------------|
| | Max Load: 1 mN | | Max Load: 5 mN | |
| | h_{\max} (nm) | h_p (nm) | h_{\max} (nm) | h_p (nm) |
| 100 | 61 ± 1 | 25 ± 3 | 164 ± 3 | 80 ± 2 |
| 10 | 65 ± 1 | 31 ± 2 | 174 ± 2 | 89 ± 3 |
| 1 | 66 ± 1 | 27 ± 1 | 175 ± 1 | 87 ± 4 |
| 0.1 | 67 ± 4 | 20 ± 2 | 178 ± 3 | 83 ± 3 |

The bolded values indicate the decrease of the residual depth, which suggests different mode of elastic recovery or phase transformation on unloading.

is observed for max load lower than 2 mN. Moreover, in this case, SRS values for both samples are very similar.

AFM measurements of the indentation imprints made with 5 mN max load are shown in Figure 8. It should be noted that in order to highlight the pile-ups we have presented the AFM measurements in two forms. The

upper images show raw AFM images, whereas in the lower images, in order to show the pile-up patterns in more detail, the measured imprint was artificially truncated at the bottom by the thresholding operation. The thresholding is useful especially for suppressing the deep, high load imprints, as the absolute value of their

ordinates is much higher than that of the surrounding pile-ups. The AFM results show that, firstly, pile-ups are clearly visible around the imprints made in the as-deposited sample and they are not observed in the annealed sample. It indicates that due to annealing the internal stress caused by the samples preparation method has been significantly reduced. The same effect (but not so clearly visible due to samples roughness) has been observed for imprints made with lower max load. Furthermore, it should be noted that apparently, the pile-ups are higher for lower loading rates. The average height of the highest pile-up for 0.1 mN/min is equal to 3.0 ± 0.5 nm whereas for 100 mN/min to 2.4 ± 0.6 nm. Nevertheless, the pile-ups are very small and they should not affect the hardness determination from

load–displacement curves according to the Oliver–Pharr method. This assumption has been confirmed by the comparison of the hardness determined by direct measurements of the projected contact area. The discrepancy between the Oliver–Pharr method and the direct measurement was in every case lower than 4 pct which also confirms the high thermal stability of the used nanoindentation tester.

Annealing has also increased samples roughness. Parameter R_a for the as-deposited sample was equal to 0.3 ± 0.1 nm whereas for the annealed sample to 1.0 ± 0.2 .

IV. DISCUSSION

In this paper, we study size effects of hardness and strain rate sensitivity of the as-deposited and annealed PECVD amorphous silicon by nanoindentation. The increase of h_{max} with a decrease of loading rate suggests that as-deposited a-Si exhibits significant plastic flow under the nanoindentation tip. The load–displacement curves shown in Figure 5(a) support this statement. There are no discontinuities on either the loading or unloading sections of the curves. Similar behavior was previously reported by Haberl *et al.*^[7] In that work, the authors performed nanoindentation of amorphous silicon samples with a spherical indenter and they investigate the cross section of imprints with a transmission electron microscope. They did not observe any phase transformations under the indenter tip in their as-deposited sample. In contrast, the nanoindentation curves taken from annealed a-Si sample, as shown in Figure 5(b), exhibit a so-called elbow behavior on unloading for lower loading rates. The occurrence of this discontinuity has been reported previously by Kiran *et al.*^[5] or Bradby *et al.*^[33] and attributed to the transformation of (β -Sn)-Si to the PI (pressure-induced) a-Si end phase. Therefore, the presence of this distinctive feature in the unloading curve is a reliable indicator that

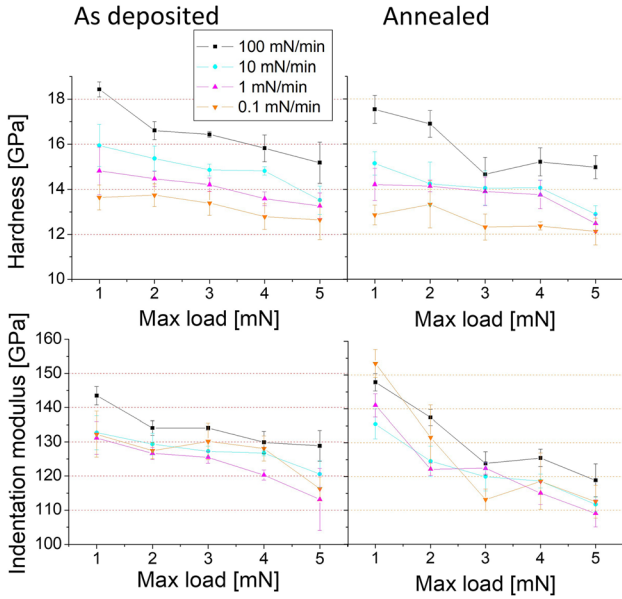


Fig. 6—The results of hardness and indentation modulus measurements.

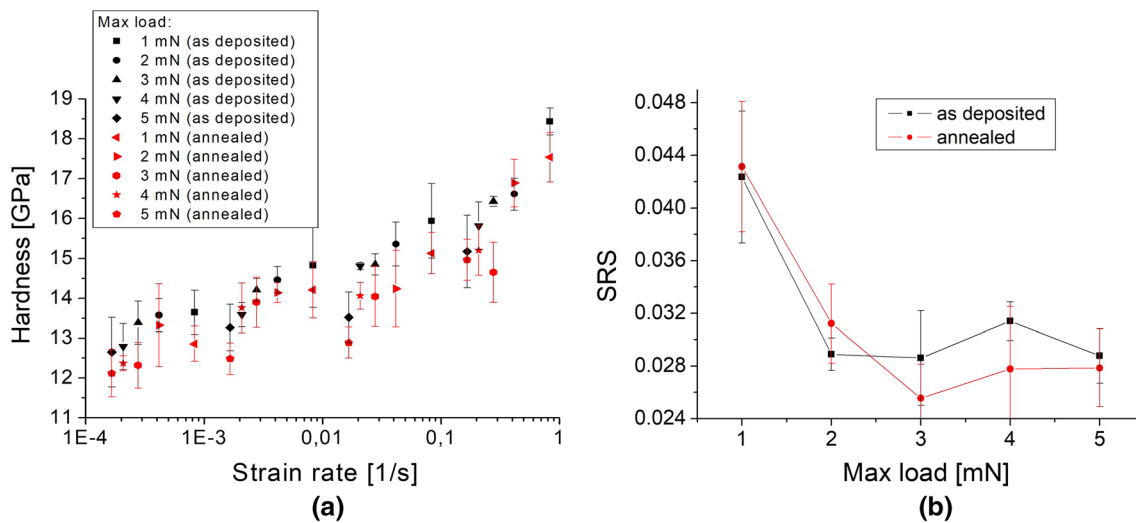


Fig. 7—(a) Plot of hardness vs indentation strain rate in which one can postulate the linear relation; (b) a plot of SRS vs max load.

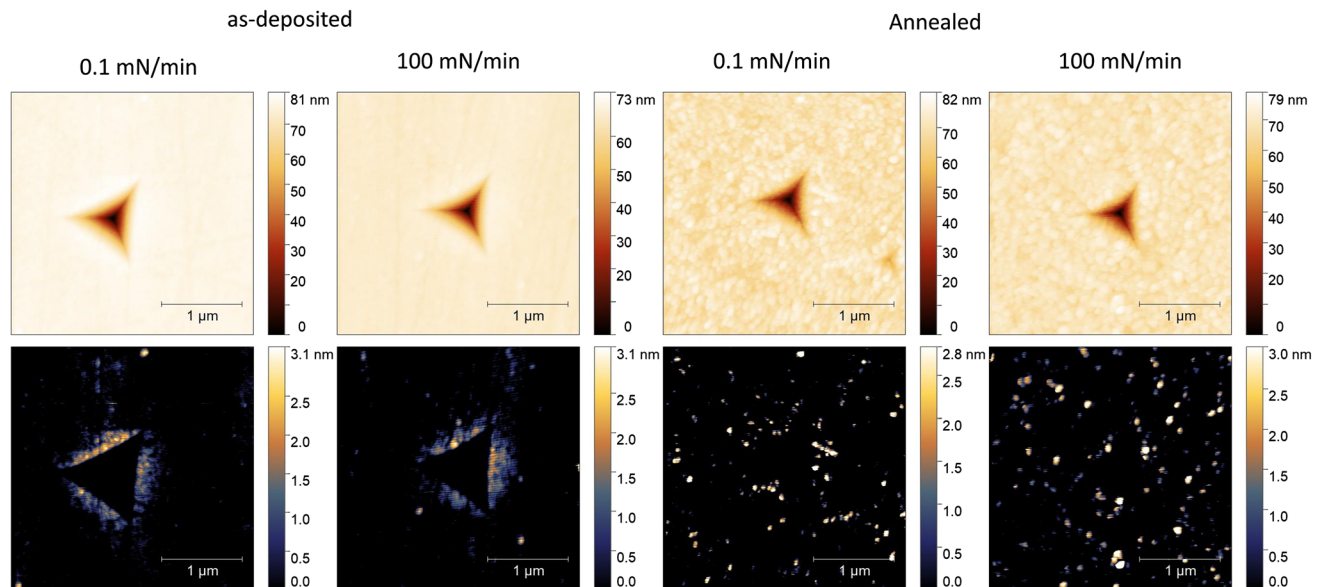


Fig. 8—AFM topography of the nanoindentation imprints and the featured pile-up patterns.

metallic (β -Sn)-Si formed on loading—a pressure-induced phase transition had occurred for lower loading rates.

These statements are also supported by the observed changes in the indentation modulus. The decrease of its measured value with the decrease of the loading rate can be explained by the plastic flow which occurs under the indenter. Furthermore, we tentatively attribute the sudden increase of the indentation modulus for the lowest loading rate to the above discussed phase transformation. However, this sudden change occurs for both samples. It is less significant for the as-deposited one, which can suggest that although the ‘elbow’ is not observed, partial phase transformation occurs in this sample. It is probable that the observation of changes in the indentation modulus is a more sensitive way to detect phase transformations in the amorphous silicon. Nevertheless, further studies are required to confirm this assumptions.

It should be noted that Haberl *et al.*^[7] loaded and unloaded their a-Si sample annealed in 450 °C with the loading rate equal to 60 and 120 mN/min and during unloading they observed a clear discontinuity called a “pop-out” instead of the elbow. Furthermore, Kiran *et al.*^[5] reported that elbows are formed for higher and pop-outs for lower unloading rates. We tentatively attribute these discrepancies to the differences in the investigated samples. In the above-mentioned papers, a-Si prepared by self-ion implantation is studied, whereas in the current study we have prepared a-Si by PECVD. The microstructure of the samples prepared by these two methods may be significantly different. In general, a-Si prepared by CVD methods usually contains voids,^[34] whereas ion implantation has been recognized as a successful technique to produce pure and voidless amorphous layers.^[35] In this paper, we have chosen to study PECVD a-Si due to its high importance for microelectronic and MEMS industries.

Furthermore, the observed differences in the behavior of a-Si under the indentation tip may also be caused also by different loading rates.

To date, the effect of loading rates on the mechanical behavior of a-Si under the indentation tip has not been studied in detail. In Figure 6(a), it is shown that the hardness significantly depends on the loading rate and it also depends on the maximal indentation load. On the other hand, high coefficients of determination estimated for a postulated linear relation between hardness and logarithm of the strain rate (Figure 7(a)) suggest that the size effect is apparent. It is probably the effect of plastic flow under the indenter, which can be described by any equation in which stress σ is related to a strain rate $\dot{\gamma}$, *i.e.*, Herschel–Bulkley equation:

$$\sigma = \sigma_0 + C\dot{\gamma}^\beta, \quad [4]$$

where σ_0 is the quasi-static flow stress and C and β are constants.

This assumption is to some extent supported by the results shown in Figure 7(b), where SRS vs max load for both samples is plotted. The constant SRS for higher loads confirms that in this range the apparent hardness size effect is caused by strain rate-dependent plastic flow. On the other hand, for the smallest loads, SRS significantly increases. This result is encouraging and should be validated and further explored for example with the use of nanoindentation strain rate jump test.^[36] Unfortunately, we do not have a facility to perform such measurements. It should be also noted that SRS is slightly smaller for the annealed sample. According to Haberl *et al.*,^[7] it may be explained by the fact that annealing of a-Si reduced the density of “defects” (broken bonds, vacancies, and interstitials-like defects). The defects facilitate the deformation through localized shear flow; hence, the as-deposited sample, with more defects, should be characterized by the higher SRS.

Finally, in a few previous papers, it was shown that annealing of voidless a-Si prepared by ion implantation leads to higher hardness due to above-mentioned reduction of the density of defects. In this research, we have observed the opposite effect. Hardness of the annealed samples is always slightly lower, independently from the experimental conditions. Furthermore, the hardness of the as-deposited sample measured for lower max loads is significantly higher than the hardness reported for a-Si produced by ion implantation.^[5,7,37] It is apparent that the behavior of PECVD a-Si is significantly different than the a-Si produced by ion implantation. It is, therefore, speculated that the higher hardness is caused by higher internal stress introduced to the sample during the manufacturing process. The annealing reduces the internal stress and, therefore, reduces hardness. High internal stress is responsible for pile-up creation during nanoindentation. In Figure 8, it is shown that the pile-ups form in the as-deposited sample and are missing in the annealed sample, which is in good agreement with the proposed explanation of the differences in hardness.

V. CONCLUSION

The measurements of dynamic mechanical properties of a-Si produced by PECVD show significant differences in comparison to the results obtained for defect-free amorphous silicon produced by ion implantation. The as-deposited PECVD a-Si exhibits significant plastic flow under the nanoindentation tip, whereas the annealed PECVD a-Si sample exhibits a so-called elbow behavior on unloading for lower loading rates, which could be attributed to the transformation of (β -Sn)-Si to the PI (pressure-induced) a-Si end phase. In contrast, the results reported in the literature for the materials made by self-ion implantation reported that elbows are formed for higher and pop-outs for lower unloading rates. We tentatively attribute these discrepancies to the fact that a-Si prepared by CVD methods usually contains voids, whereas ion implantation has been recognized as a successful technique to produce pure and voidless amorphous layers. Another difference is the fact that in this paper we have measured lower hardness for the annealed sample. This effect is opposite to the behavior of the a-Si produced by self-ion implantation described in the literature, in which hardness usually increases after annealing. In this case, the possible explanation is the reduction of internal stress after annealing.

Furthermore, we have also shown that the hardness of PECVD a-Si significantly depends on the loading rate and on the maximal indentation load. These results presented in this paper may be important especially for MEMS/NEMS industry in which this material is often used. Nevertheless, an important question for further studies is to explain the increase of SRS for small indentation depths and to study PECVD a-Si with much higher strain rates.

ACKNOWLEDGMENTS

The present research was partially supported by the Polish National Science Centre, Grant 2015/19/D/ST8/03200.

OPEN ACCESS

This article is licensed under a Creative Commons Attribution 4.0 International License, which permits use, sharing, adaptation, distribution and reproduction in any medium or format, as long as you give appropriate credit to the original author(s) and the source, provide a link to the Creative Commons licence, and indicate if changes were made. The images or other third party material in this article are included in the article's Creative Commons licence, unless indicated otherwise in a credit line to the material. If material is not included in the article's Creative Commons licence and your intended use is not permitted by statutory regulation or exceeds the permitted use, you will need to obtain permission directly from the copyright holder. To view a copy of this licence, visit <http://creativecommons.org/licenses/by/4.0/>.

REFERENCES

1. R.M.R. Pinto, P. Brito, V. Chu, and J.P. Conde: *J. Microelectromech. Syst.*, 2019, vol. 28, pp. 390–400.
2. J. Gaspar, A. Gualdino, B. Lemke, O. Paul, V. Chu, and J.P. Conde: *J. Appl. Phys.*, 2012, vol. 112, art. no. 024906.
3. B. Haberl, M. Guthrie, D.J. Sprouster, J.S. Williams, and J.E. Bradby: *J. Appl. Crystallogr.*, 2013, vol. 46, pp. 758–68.
4. Y.B. Gerbig, C.A. Michaels, J.E. Bradby, B. Haberl, and R.F. Cook: *Phys. Rev. B*, 2015, vol. 92, art. no. 214110.
5. M. Kiran, B. Haberl, J.S. Williams, and J.E. Bradby: *J. Appl. Phys.*, 2014, vol. 115, art. no. 113511.
6. B. Haberl, A.C.Y. Liu, J.E. Bradby, S. Ruffell, J.S. Williams, and P. Munroe: *Phys. Rev. B*, 2009, vol. 79, art. no. 155209.
7. B. Haberl, J.E. Bradby, M.V. Swain, J.S. Williams, and P. Munroe: *Appl. Phys. Lett.*, 2004, vol. 85, pp. 5559–61.
8. Z. Wu, J. Thou, W. Chen, J. Shen, C. Lv, and Y.Y. Qi: *Ceram. Int.*, 2015, vol. 41, pp. 11632–36.
9. Z.W. Chen and N. Brandon: *Ceram. Int.*, 2016, vol. 42, pp. 8316–24.
10. D. Naujoks *et al.*: *Acta Mater.*, 2017, vol. 138, pp. 100–10.
11. S. Kauffmann-Weiss, S. Hahn, C. Weigelt, L. Schultz, M.F.X. Wagner, and S. Fahler: *Acta Mater.*, 2017, vol. 132, pp. 255–63.
12. J.E. Bradby, J.S. Williams, J. Wong-Leung, M.V. Swain, and P. Munroe: *J. Mater. Res.*, 2001, vol. 16, pp. 1500–507.
13. S. Wong *et al.*: *J. Appl. Phys.*, 2019, vol. 126, art. no. 105901.
14. J.I. Jang, M.J. Lance, S.Q. Wen, T.Y. Tsui, and G.M. Pharr: *Acta Mater.*, 2005, vol. 53, pp. 1759–70.
15. T. Juliano, Y. Gogotsi, and V. Domnich: *J. Mater. Res.*, 2003, vol. 18, pp. 1192–1201.
16. Y.M. Wei, Z.G. Lu, K.H. Hu, X.Y. Li, and P.J. Li: *Ceram. Int.*, 2018, vol. 44, pp. 11702–10.
17. D. Ghosh, M. Banda, J.E. John, and D.A. Terrones: *Scripta Mater.*, 2018, vol. 154, pp. 236–40.
18. Y. Wei: *J. Mater. Sci.*, 2007, vol. 42, pp. 1709–27.
19. J. Fornell *et al.*: *Acta Mater.*, 2010, vol. 58, pp. 6256–66.
20. C. Liu, V. Roddatis, P. Kenesei, and R. Maass: *Acta Mater.*, 2017, vol. 140, pp. 206–16.

21. P.Y. Zhao, J. Li, J. Hwang, and Y.Z. Wang: *Acta Mater.*, 2017, vol. 134, pp. 104–15.
22. J.L. Wang, L.X. Wu, X. Chen, W.J. Zhuo, and G.F. Wang: *Sensors Actuators A*, 2018, vol. 276, pp. 11–16.
23. D.A. Antartis, R.N. Mott, and I. Chasiotis: *Mater. Des.*, 2018, vol. 144, pp. 182–91.
24. H.K. Malik, S. Juneja, and S. Kumar: *J. Theor. Appl. Phys.*, 2019, vol. 13, pp. 107–13.
25. A. Soman, U. Nsofor, U. Das, T.Y. Gu, and S. Hegedus: *ACS Appl. Mater. Interfaces*, 2019, vol. 11, pp. 16181–16190.
26. M. Chmielewski *et al.*: *Int. J. Refract Metal Hard Mater.*, 2016, vol. 59, pp. 78–86.
27. J. Nohava, N.X. Randall, and N. Conte: *J. Mater. Res.*, 2009, vol. 24, pp. 873–82.
28. Y. Liu, J. Hay, H. Wang, and X. Zhang: *Scripta Mater.*, 2014, vol. 77, pp. 5–8.
29. D. Pan, A. Inoue, T. Sakurai, and M.W. Chen: *Proc. Natl. Acad. Sci. USA*, 2008, vol. 105, pp. 14769–772.
30. J.G. Swadener, E.P. George, and G.M. Pharr: *J. Mech. Phys. Solids*, 2002, vol. 50, pp. 681–94.
31. S.J. Bull, T.F. Page, and E.H. Yoffe: *Philos. Mag. Lett.*, 1989, vol. 59, pp. 281–88.
32. D.E. Stegall and A.A. Elmustafa: *Metall. Mater. Trans. A*, 2018, vol. 49A, pp. 4649–58.
33. J.E. Bradby, J.S. Williams, J. Wong-Leung, M.V. Swain, and P. Munroe: *Appl. Phys. Lett.*, 2000, vol. 77, pp. 3749–51.
34. S. Saitoh, T. Sugii, H. Ishiwara, and S. Furukawa: *Jpn. J. Appl. Phys.*, 1981, vol. 20, pp. L130–L132.
35. S. Roorda *et al.*: *Phys. Rev. B*, 1991, vol. 44, pp. 3702–25.
36. V. Maier, K. Durst, J. Mueller, B. Backes, H.W. Hoppel, and M. Goken: *J. Mater. Res.*, 2011, vol. 26, pp. 1421–30.
37. S.K. Bhuyan *et al.*: *MRS Commun.*, 2012, vol. 2, pp. 9–12.

Publisher's Note Springer Nature remains neutral with regard to jurisdictional claims in published maps and institutional affiliations.